Pulsed Laser Micro Polishing: Surface Prediction Model

Madhu Vadali[1], Chao Ma[2], Neil A. Duffie[3], Xiaochun Li[4], and Frank E. Pfefferkorn[5,*]

[1]Madhu Vadali; Mechanical Engr., University of Wisconsin - Madison; e-mail: vadali@wisc.edu
[2]Chao Ma; Mechanical Engr., University of Wisconsin - Madison; e-mail: cma25@wisc.edu
[3]Neil A. Duffie; Mechanical Engr., University of Wisconsin - Madison; e-mail: duffie@engr.wisc.edu
[4]Xiaochun Li; Mechanical Engr., University of Wisconsin - Madison; e-mail: xcli@engr.wisc.edu
[5]Frank E. Pfefferkorn; Mechanical Engr., University of Wisconsin - Madison; e-mail: pfefferk@engr.wisc.edu

ABSTRACT

This project is focused on developing physics-based models to predict the outcome of pulsed laser micro polishing (PLµP). Perry et al. [1-3] have modeled PLµP as oscillations of capillary waves with damping resulting from the forces of surface tension and viscosity and a one-dimensional spatial frequency domain analysis was proposed. They have also proposed a critical spatial frequency, f_{cr}, above which a significant reduction in the amplitude of the spatial Fourier components is expected. The current work extends the concept of critical frequency to two dimensional spatial frequency analysis of PLµP. We propose a physics-based prediction methodology to predict the spatial frequency content and surface roughness after polishing, given the features of the original surface, the material properties, and laser parameters used for PLµP.

The proposed prediction methodology was tested using PLµP line polishing data for stainless steel 316L and area polishing results for pure Nickel, Ti6Al4V, and Al-6061-T6. The predicted average surface roughnesses were within 10% to 12% of the values measured on the polished surfaces. The results show that the critical frequency continues to be a useful predictor of polishing results in the 2-D spatial frequency domain. The laser processing parameters, as represented by the critical frequency, and the initial surface texture can be used to predict the final surface roughness before actually implementing PLµP.

INTRODUCTION

Perry et al. [1-3] have demonstrated that pulsed laser micro-polishing (PLµP) with pulse durations of 300-650 ns and a spot size of 60 µm is a method by which the surface roughness of microfabricated and micro milled parts can be effectively reduced. Improved surface finish and smoothness can be achieved on *select areas* of different metallic surfaces, produced by meso/micro-manufacturing processes, which is difficult via other methods (like mechanical polishing, electropolishing and chemical mechanical polishing) as the feature sizes are approaching the same magnitude as the surface roughness [4-8]. Past research on laser induced surface modification and surface finish also indicate that reduction surface is also possible at pulse durations less than 200 ns and spot sizes of few hundreds of microns.[9, 10]. Most recent research includes laser induced surface finish of titanium for bio-implants[11, 12] and micro-roughness reduction of tungsten films in the IC industry[13].

In PLµP, laser pulses irradiate the surface. Each pulse results in melting followed by damped oscillations of the melted surface due to the forces of surface tension and viscosity. If the oscillations damp out within the time that the surface is molten, a smoother surface will result upon solidification [16, 17]. Analytical models were proposed to describe the dynamics of the melt pool [10-12]. These models are based on spatial Fourier analysis of the surfaces and examination of Navier-Stokes equation for each Fourier component. In the present work, we extend these analytical models and numerical models of Perry et al. [1-3] to two dimensions and use the same to predict the surface finish, given the initial surface conditions.

Perry et al. [1-3] have proposed a critical frequency, f_{cr}, which describes the cutoff point in the spatial frequency content of the surface, above which a significant reduction in the amplitude is expected. The critical frequency is a function of the duration of the molten state. Experimental studies using a variety of materials (stainless steel 316L, nickel, Ti6Al4V and Al-6061-T6), initial surface roughness (70-190 nm) and pulse durations (300 to 5000 ns) have confirmed the ability of the critical frequency to predict which surface features (asperities) will experience significant reductions in amplitude, i.e., polishing.

In the current work, we aim to (1) extend the concept of the critical frequency to 2-D spatial frequency analysis and (2) use it to predict the polished surface topography and roughness resulting from PLµP. The ability to predict the two-dimensional surface topography and roughness of the polished surface is expected to be a significant tool in the selection of laser parameters based on the requirements of the final surface. Experimental results are presented that allow predicted surface spatial frequency content and roughness to be compared with empirical surface spatial frequency content and roughness for micro end milled surfaces on three different metals: nickel, Ti6Al4V and Al-6061-T6.

PROCESS MODEL

Predicting the outcome of PLµP requires a model of how the surface behaves when it is molten. This has been accom-

.* corresponding author

plished by integrating an analytical fluid flow model and a numerical heat transfer model.

A. FLUID FLOW MODEL

When a laser pulse of sufficient energy is incident on a surface, the surface asperities and some depth of metal below the surface melt. The molten asperities (i.e., roughness features) become regions of high surface tension because of their smaller radius of curvature. These molten asperities have small amplitude to wavelength ratios and can be modeled as capillary waves. The surface tension forces acting on these molten asperities introduce sinusoidal oscillations on the surface, and the amplitude of these oscillations will decay due to viscosity. In the current model, it is assumed that these oscillations correspond to standing waves. Gravity forces can be neglected at these scales.

2-D spectral analysis techniques are used to model the geometry of the surface [18]. The surface is transformed into the corresponding spatial Fourier components that are used in modeling. Landau and Lifshitz [19] have shown that the amplitude, ζ, of a spatial frequency component decays exponentially with time:

$$\zeta(t) = \zeta(0)\, e^{-\gamma t} \qquad (1)$$

where, γ, the coefficient of damping, for a given Fourier component of wave number κ is

$$\gamma = \frac{2\,\mu\,\kappa^2}{\rho} \qquad (2)$$

where, μ is the dynamic viscosity and ρ is the density. The wave number, κ, can be expressed in terms of spatial frequencies, f_x and f_y, as

$$\kappa = 2\,\pi\,\left(f_x\,\boldsymbol{i} + f_y\,\boldsymbol{j}\right) \qquad (3)$$

The amplitude of interest in PLμP is the amplitude of a spatial frequency component at the surface of the melt pool at the maximum melt duration, $t_{m\text{-}max}$. Therefore, Eq. (1) can be rewritten as

$$\zeta(t_{m\text{-}max}) = \zeta(0)\, e^{-\gamma t_{m\text{-}max}} \qquad (4)$$

which gives the final amplitude for a given spatial frequency component. Using Eqs. (2) and (3), this result can be generalized for all spatial frequencies, f_x and f_y, as

$$\zeta(f_x,f_y)_{polished} = \zeta(f_x,f_y)_{unpolished}\, e^{-\gamma(f_x,f_y)\, t_{m\text{-}max}} \qquad (5)$$

where,

$$\gamma(f_x, f_y) = \frac{8\pi^2\mu\left(f_x^2 + f_y^2\right)}{\rho} \qquad (6)$$

Perry et al [1-3] have shown that knowledge of the maximum melt duration, $t_{m\text{-}max}$, can be used to determine the minimum critical frequency, f_{cr}, above which there should be a significant reduction in amplitude of the spatial frequency content of a surface and its asperities. The critical frequency is

$$f_{cr} = \left(\frac{\rho}{8\pi^2\mu t_{m\text{-}max}}\right)^{\frac{1}{2}} \qquad (7)$$

The melt pool is assumed to axisymmetric, hence the critical frequency is assumed to be identical in the x and y directions. Using Eqs. (5), (6) and (7), the amplitude of the surface at spatial frequency f_x and f_y, $\zeta(f_x,f_y)$, after solidification (i.e., at the end of $t_{m\text{-}max}$) can be predicted using

$$\zeta(f_x,f_y)_{polished} = \zeta(f_x,f_y)_{unpolished}\, e^{-\left[(f_x/f_{cr})^2 + (f_y/f_{cr})^2\right]} \qquad (8)$$

This is a special case of a low-pass Gaussian filter, and prediction of the final surface can be viewed as a filtering process with the break frequency at the critical frequency. Note that the mathematics behind 2-D spectral analysis (2-D Fourier analysis) results in spectral content corresponding to negative frequencies. Physically, these negative spatial frequencies have no significance. Hence, all further discussion will be confined to positive spatial frequencies in both x and y directions. Fig. 1 illustrates the spatial filter confined to the positive frequencies.

With knowledge of the spatial frequency content of the surface before polishing and an estimate of the critical frequency obtained from Eq. (7), Eq. (8) can be used to predict the spatial frequency content of the laser polished surface. The average surface roughness can then be calculated from the predicted surface profile. Determining the critical frequency requires an estimate of the maximum melt duration. A transient, two-dimensional axisymmetric heat transfer model of pulsed laser melting has been developed for this purpose.
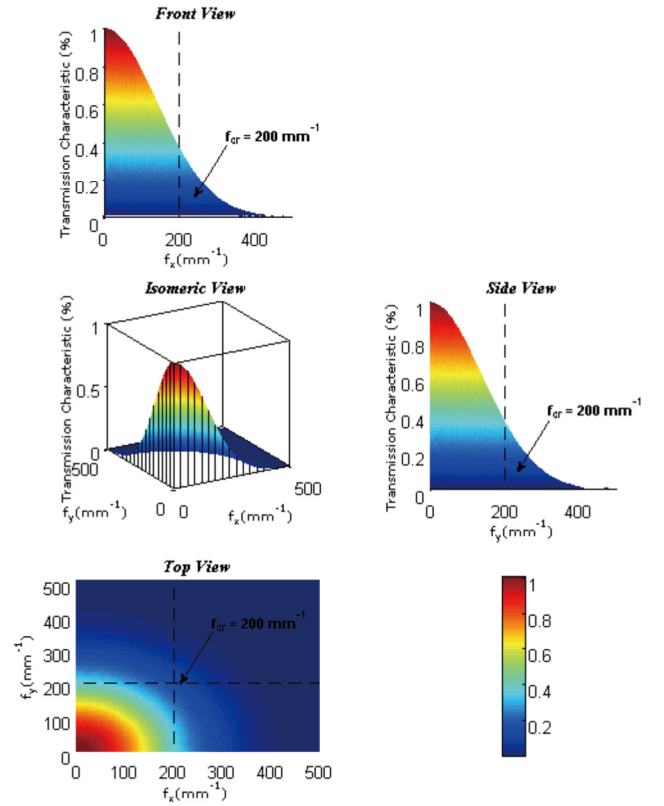

Fig. 1: First quadrant (positive spatial frequencies) section of a typical 2-D low pass filter described in Eq. (8).

B. HEAT TRANSFER MODEL

Perry et al. [1-3] used a one-dimensional finite element model to simulate melting due to a single laser pulse in which it was assumed that [20]

$$\chi \, t_{pulse} << r^2 \qquad (9)$$

where χ is the thermal diffusivity, t_{pulse} is the laser pulse duration, and r is the laser spot radius. The ability of this one-dimensional model to accurately estimate $t_{m\text{-}max}$ diminishes at higher pulse durations. Therefore, a transient, two-dimensional axisymmetric model was developed. To simplify the model, polishing was assumed to occur in an inert atmosphere, the workpiece was assumed to be homogenous and isotropic, reflectivity of the melt was not considered, convection and radiation were assumed to be negligible, and the initial temperature of the workpiece was assumed to be room temperature: 298K.

The physical properties of stainless steel 316L, Nickel, Ti6Al4V and Al-6061-T6 [21] used in the finite element analysis software (ANSYS) include enthalpy change ΔH and thermal conductivity k. The properties of stainless steel 316L were not available in the literature hence the properties of stainless steel 316 were used. Considering the phase change in the melting process, the total enthalpy change ΔH was represented by a sum of sensible heat Δh and latent heat content ΔL, i.e., $\Delta H = \Delta h + \Delta L$ [22]. The sensible heat h can be expressed as $\Delta h = \int_{298}^{T} C_p \, dT$, where C_p is the specific heat and T is the temperature. The latent heat content ΔL is given as $\Delta L = L \cdot F_L$, where L is the latent heat of melting. The liquid fraction F_L was assumed to vary linearly with temperature [22]:

$$F_L = \begin{cases} 1 & T > T_L \\ \dfrac{T - T_S}{T_L - T_S} & T_S \leq T \leq T_L \\ 0 & T < T_S \end{cases} \qquad (10)$$

where T_L and T_S are the liquidus and solidus temperatures, respectively. However, pure Nickel does not change phase over a range of temperatures: i.e., liquidus = solidus = melting temperature. This results in a rapid increase in enthalpy as the temperature increases during phase change, which in turn can cause convergence problems in numerical solutions. To accommodate this nonlinearity, an arbitrary solidification range of 6 K was introduced [23], which is 0.3% of the melting temperature.

The heat flux incident on the workpiece was modeled as spatially uniform (flat top) and Gaussian in the time domain. The laser pulse duration was defined as full width at half maximum (FWHM) of the Gaussian function.

PREDICTION METHODOLOGY

The proposed method for surface profile and roughness prediction is shown in Fig. 2 and consists of the following steps:

Step 1: Initial surface data acquisition and pre-processing

The first step is to obtain the surface height data of the initial (unpolished) surface using an appropriate measurement technique. In the current work, all surface measurements were made using a white-light interferometer (Zygo® NewView™ 6300). The interferometry technique also captures the surface curvature/form. Least squared error method was used to compute the mean plane from the surface height data and was removed.

Step 2: Estimation of process parameters

The two process parameters required for the prediction model are the maximum melt duration, $t_{m\text{-}max}$ and the critical frequency, f_{cr}. The two-dimensional axisymmetric heat transfer model described above was used to numerically estimate the maximum melt duration. Using this result and Eq. (7), the critical frequency was predicted. The physical parameters used are listed in Table 1.

Table 1: Physical properties of stainless steel 316, nickel, Ti6Al4V, 6061-T6 and aluminum[21]

Material	Dynamic Viscosity, μ (mPa.s)	Density, ρ (kg/m3)
Stainless Steel 316	8.00	6881
Nickel	4.70	7850
Ti6Al4V	3.23	3917
Al-6061-T6	1.15	2415

Step 3: Spatial domain filtering

This step involves predicting the spatial frequency spectrum of the polished surface using the spatial frequency spectrum of the initial unpolished surface. The unpolished spatial frequency spectrum was computed using two dimensional Fast Fourier analysis of the digital surface height data, and the low pass spatial filter described in Eq. (8) was applied. This gives the prediction of spatial frequency content of the polished surface.

Step 4: Characterization of the predicted polished surface

Roughness average, S_a, and root mean square (rms) roughness, S_q, and were computed [24]. The surface height data, $Z(x, y)$, is obtained by inverse Fourier transformation of the predicted polished surface spatial frequency content.

EXPERIMENTAL METHODS AND SETUP

The accuracy of the prediction methodology was compared to a variety of experimental data sets. In the current paper, prediction results on four materials: stainless steel 316L, Nickel, Ti6Al4V and Al-6061-T6, are reported and are compared to the actual PLμP results. The experimental surfaces on stainless steel 316L and Ti6Al4V were produced using micro end milling while the surfaces on Nickel and Al 6061-T6 were produced with abrasive media (i.e., 400, 600, 800, and 1200 grit abrasive pads). These processes were chosen because they result in surface topographies with rich frequency content.

The basic experimental setup is illustrated in Fig. 3. A 1064nm, 250 W (CW) Nd:YAG laser (Lee Lasers, Model: 8250MQ) was used for experimentation. The laser was directed by static mirrors into a scan head (ScanLab Hurry-Scan 14 mm) to allow for high-speed, two-dimensional scanning at beam velocities of up to 1.5 m/s. The scan head was controlled by a ForeSight control card from LasX Industries and had an f-theta objective (Linos f-theta-Ronar, Model: 4401-302-000-20/21) with a focal length of 100 mm. A z-axis manual stage was used to adjust the laser spot size (i.e., fluence incident on the sample) and to accommodate samples of varying thickness.
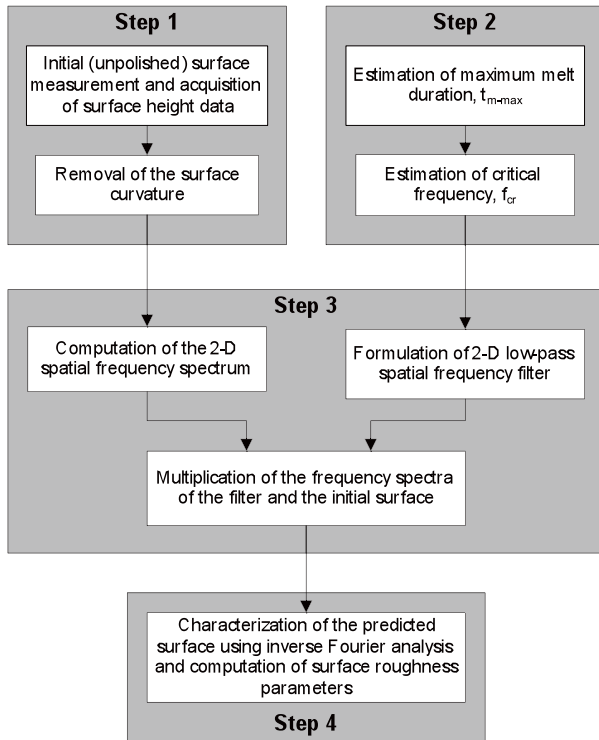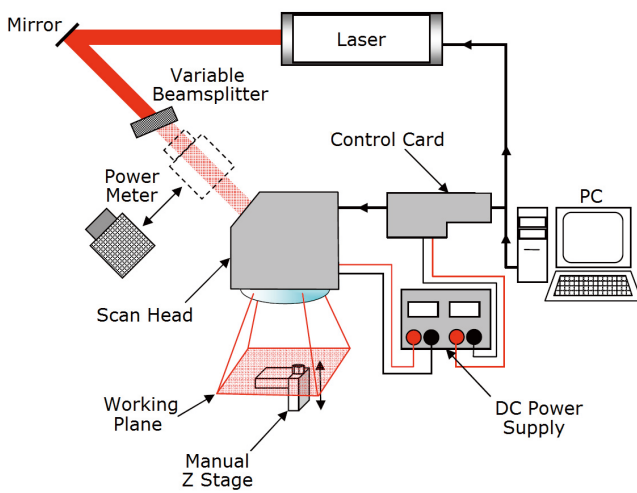

Fig. 2: PLµP surface prediction method

Fig. 3: Experimental setup

RESULTS

A. LINE POLISHING RESULTS

Initially, the prediction methodology was assessed using one-dimensional analysis. Line profile data of the rough unpolished surface was obtained from a micro end milled stainless steel 316 L sample using white-light interferometry. The average roughness, R_a, was calculated to be 183 nm. PLµP was carried out using a 1070 nm wavelength, 50 W CW/modulated fiber laser, producing 5000 ns pulses. The melt duration was estimated to be 6820 ns and the critical frequency was found to be approximately 40 mm^{-1}. Fig. 4 shows the surface model, and Fig. 5 shows the surface intensity map obtained using a white-light interferometer. PLµP reduced the average roughness to 84.7 nm, while the proposed methodology predicted an R_a of 76.6 nm after PLµP.

Fig. 6 shows the spatial frequency spectra, obtained by Fourier transformation, of the polished and the unpolished line profile data from Fig. 5. Also shown is the filtered spatial frequency spectrum, which represents the frequency content predicted for the polished surface. The predicted spectrum compares well with the spectrum of the actual polished surface.
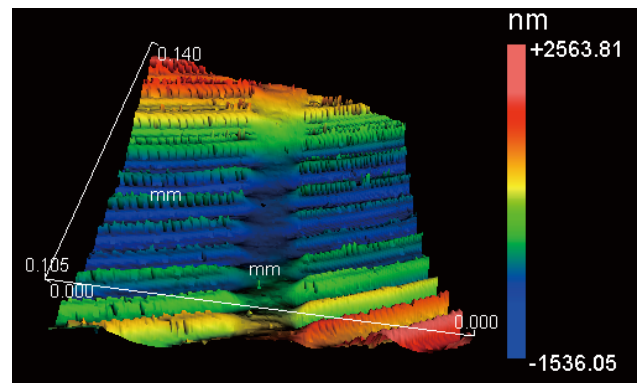

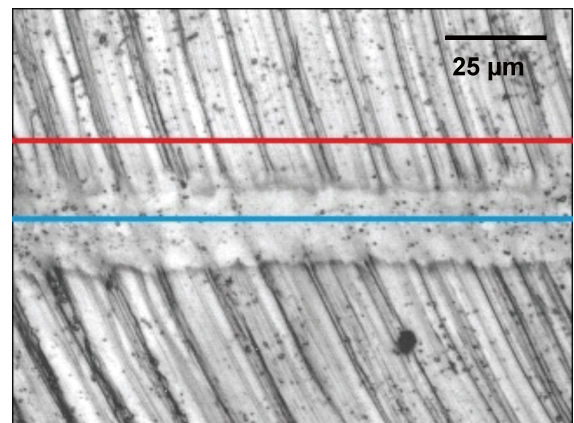*Fig. 4: Surface model of the polished stainless steel 316L sample*

Fig. 5: Surface intensity map of stainless steel 316L sample with polished (blue) and unpolished (red) lines
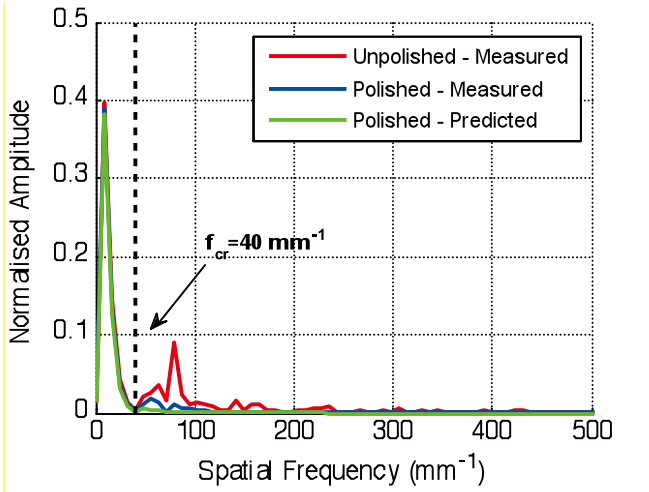
Fig. 6: Spatial frequency plots of the original (unpolished), actual (polished-measured) and predicted (polished-predicted) line profiles on stainless steel 316L sample

B. AREA POLISHING RESULTS

Area polishing results for three different samples now will be discussed. While the initial surfaces on Ti6Al4V were produced through micro end milling, the surfaces on Nickel and Al-6061-T6 were produced by abrasive media. They were polished using 650 ns laser pulses from a Nd:YAG laser at 1064 nm wavelength. The polishing was done at fluence values specific to each material.

Nickel

PLμP was performed on a macro scale ground Nickel surface. A 500 μm x 500 μm area was polished with the laser beam following a square zig-zag trajectory. The laser was pulsed at 4 kHz corresponding to a pulse duration of 650 ns. The maximum melt duration estimated using the two-dimensional heat transfer model is 994 ns (Table 2). This was used in Eq. (7) to predict the critical frequency, which was found to be 145 mm^{-1}.

Table 2: Heat transfer model based estimations of maximum melt duration and critical frequency

Material	Pulse duration, t_{pulse} (ns)	Maximum melt duration, t_{m-max} (ns)	Critical frequency, f_{cr} (mm^{-1})
Stainless steel 316L	5000	6820	40
Nickel	650	994	145
Ti6Al4V	650	1164	115
Al-6061-T6	650	2335	107

Figs. 7(a) and 7(b) show the 3D surface height data of the unpolished and polished regions (350 μm x 265 μm) measured using the white light interferometer. Fig. 7(c) shows polished surface height data predicted using the proposed prediction methodology. Note that the measurements of unpolished surface height data and polished surface height data were made at different locations on the sample surface. This will not have a significant effect on the computation of the roughness parameters because the errors generally

roughness parameters because the errors generally average out.

S_a calculated from the measured surface height data reduced from an initial value of 191.3 nm to 146.8 nm, while the proposed methodology predicts a final roughness of 130.6 nm. The error in prediction can be partly attributed to the fact that the prediction is based on the unpolished surface height data which is measured at a different location than the polished surface height data. Fig. 8 shows the 2-D spectral content of the unpolished, polished and the predicted surfaces along with the critical frequency. Note that the amplitude of the frequencies above f_{cr} is significantly reduced.

Ti6Al4V

The prediction methodology was next evaluated with micro end milled surfaces created on Ti6Al4V. The unpolished and polished surface height data were obtained using the white light interferometer [2]. The 3D surface heights are shown in Fig. 9 and the spatial frequency plots in Fig. 10. It can be seen that the predicted surface heights and the frequency spectrum closely matches the actual polished heights and the spectrum respectively. The maximum melt duration was estimated to be 1164 ns corresponding to 650 ns pulse duration (Table 2). The critical frequency was found to be 115 mm^{-1}. Spatial filtering was performed with the estimated f_{cr} as described in Step 3 of the prediction methodology. The initial average surface roughness was 181.2 nm and was reduced to 82.2 nm through PLμP. The average surface roughness was predicted to be 89.9 nm (see Table 3). Note again that the actual surface height profile is different from the predictions because the prediction is based on the unpolished surface profile, measured at a different location than the polished surface.

Al-6061-T6

The final material used to assess the proposed prediction methodology is Al-6061-T6. The initial surface was produced using macro scale grinding process resulting in an initial average roughness of 191.7 nm. PLμP was carried out again at 650 ns long pulse and the maximum melt duration was estimated to be 2335 ns. The critical frequency was found to be 107 mm^{-1}. The roughness average of the polished surface calculated from the measured surface heights (Fig. 11(b)) is 130.8 nm while the prediction is 115 nm. Fig. 11 shows 3-D surface heights of the measured unpolished and polished surfaces along with the predictions. Fig. 12 shows the spatial frequency spectra, obtained by 2-D Fourier transformation, of the unpolished and the unpolished surface height data from Fig. 11. Also shown is the filtered spatial frequency spectrum, which represents the frequency content predicted for the polished surface. Both the predicted surface heights and the frequency spectrum compare well with the surface heights and the corresponding frequency spectrum of the actual polished surface.
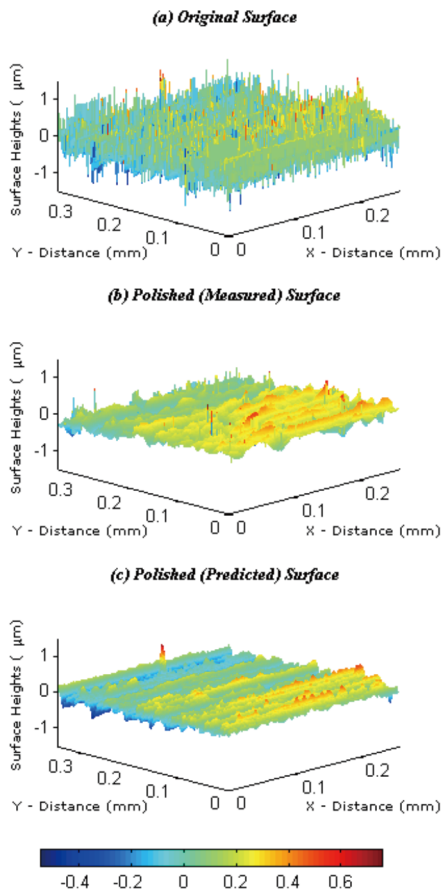
(a) Original Surface

(b) Polished (Measured) Surface

(c) Polished (Predicted) Surface

Fig. 7: Original unpolished, polished measured and polished predicted, 3-D surface height data of nickel

(a) Original Surface

(b) Polished (Measured) Surface

(c) Polished (Predicted) Surface

Fig. 9: Original unpolished, polished measured and polished predicted, 3-D surface height data of Ti6Al4V

(a) Original Surface [Front View]

(b) Original Surface [Side View]

(c) Polished (Measured) Surface [Front View]

(d) Polished (Measured) Surface [Side View]

(e) Polished (Predicted) Surface [Front View]
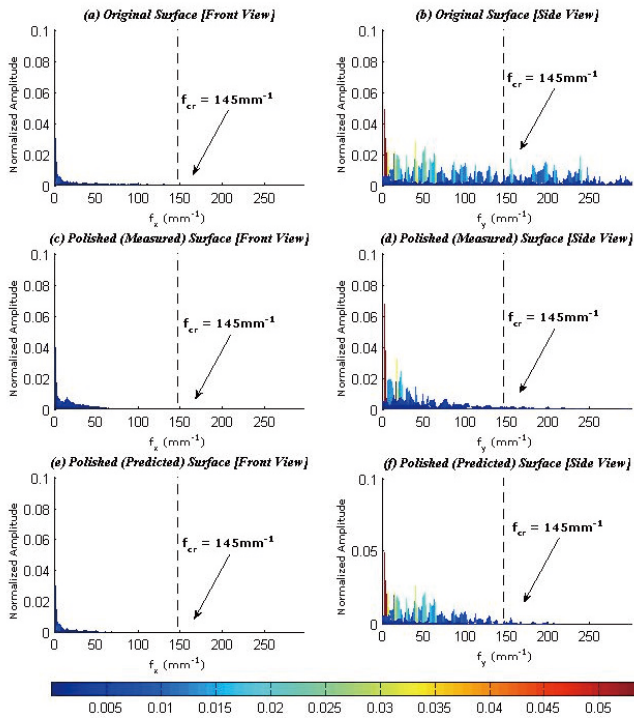
(f) Polished (Predicted) Surface [Side View]

Fig. 8: 2-D spatial frequency plots of the original unpolished, polished measured and polished predicted surface on nickel

(a) Original Surface [Front View]

(b) Original Surface [Side View]

(c) Polished (Measured) Surface [Front View]

(d) Polished (Measured) Surface [Side View]

(e) Polished (Predicted) Surface [Front View]

(f) Polished (Predicted) Surface [Side View]

Fig. 10: 2-D spatial frequency plots of the original unpolished, polished measured and polished predicted surface on Ti6Al4V

336

(a) Original Surface

(b) Polished (Measured) Surface
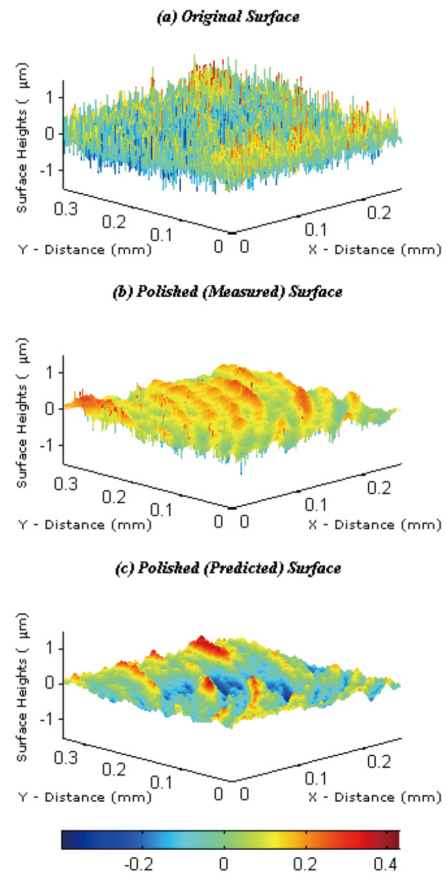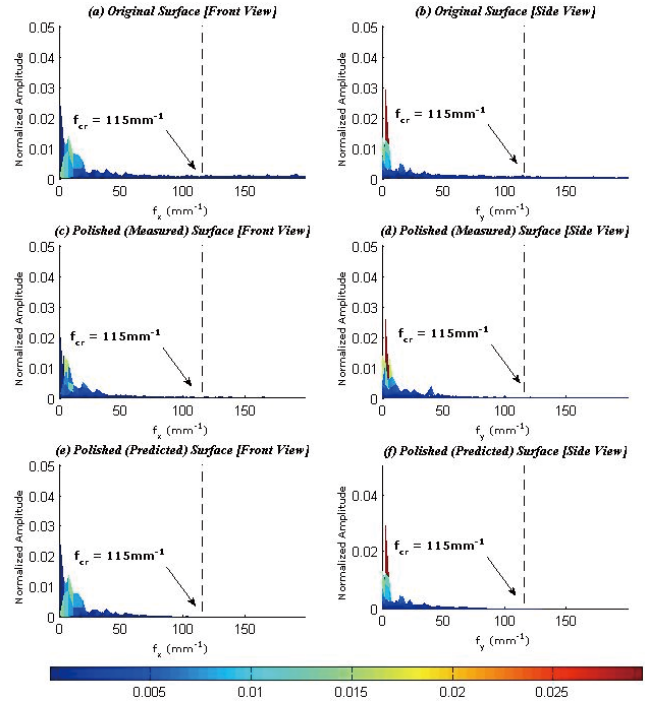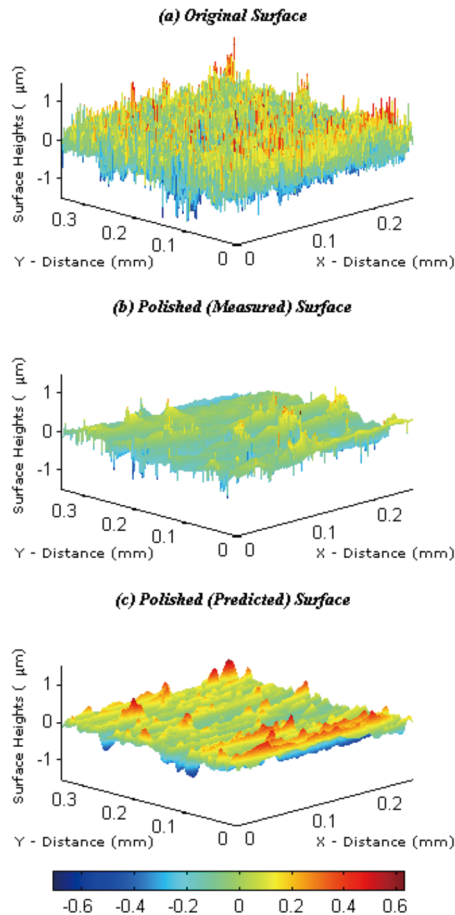
(c) Polished (Predicted) Surface

Fig. 11: Original unpolished, polished measured and polished predicted, 3-D surface height data of Al-6061-T6
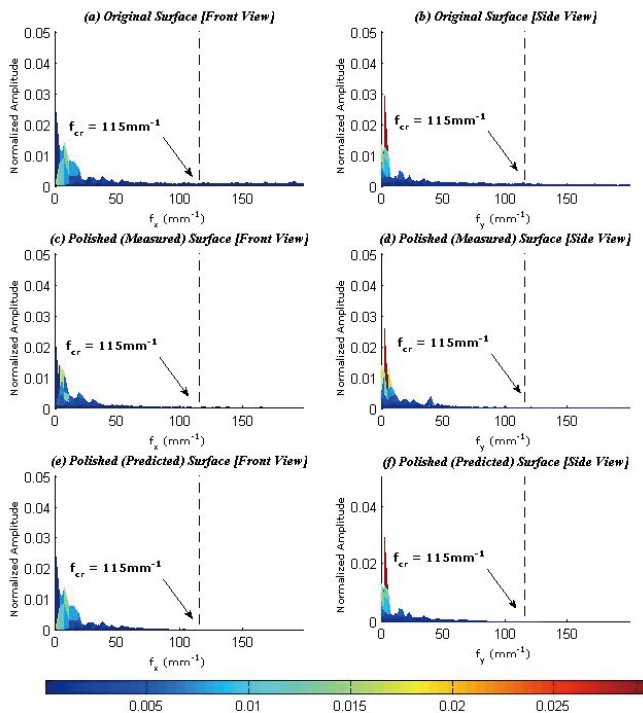

Fig. 12: 2-D spatial frequency plots of the original unpolished, polished measured and polished predicted surface on Al-6061-T6

CONCLUSIONS

An analytical fluid dynamic model for capillary waves and a numerical heat transfer model were developed and combined to predict the spatial frequency content of the surface resulting from PLµP process, and also predict the resulting roughness. The prediction methodology was initially applied on surface line profiles and was validated on stainless steel. Later, it was evaluated, using 2-D Fourier analysis, for area finishing through PLµP. The predictions were made on three different materials: Nickel, Ti6Al4V and Al-6061-T6. In each case, the roughness predicted for the polished surface was similar to the actual polishing results. In the case of Nickel, the roughness parameters were underestimated by approximately 16 nm corresponding to an error of 11%, while Ti6Al4V roughness was overestimated by approximately 8 nm, or 10%. For Al-6061-T6, the roughness parameters were under-estimated by 10-15 nm. This corresponds to an error of 12%. These results indicate that the proposed prediction methodology can quickly and effectively predict polishing results for a variety of materials despite the numerous assumptions that are made.

Table 3: 2-D surface roughness parameters of unpolished, polished and predicted surfaces.

Material	Unpolished	Polished	Predicted
Roughness average, S_a (nm)			
Nickel	191.3	146.8	130.6
Ti6Al4V	181.2	82.2	89.9
Al-6061-T6	191.7	130.8	115.0
Root mean square roughness, S_q (nm)			
Nickel	252.1	180.3	163.0
Ti6Al4V	238.1	112.0	113.9
Al-6061-T6	257.5	162.2	150.9

REFERENCES

[1] T. L. Perry, D. Werschmoeller, N. A. Duffie, X. C. Li, and F. E. Pfefferkorn, "Examination of Selective Pulsed Laser Micropolishing on Microfabricated Nickel Samples Using Spatial Frequency Analysis," Journal of Manufacturing Science and Engineering-Transactions of the Asme, vol. 131, no. 2, 2009.

[2] T. L. Perry, D. Werschmoeller, X. Li, F. E. Pfefferkorn, and N. A. Duffie, "Pulsed laser polishing of micro-milled Ti6Al4V samples," Journal of Manufacturing Processes, vol. 11, no. 2, 2009, pp. 74-81.

[3] T. L. Perry, D. Werschmoeller, X. C. Li, F. E. Pfefferkorn, and N. A. Duffie, "The Effect of Laser Pulse Duration and Feed Rate on Pulsed Laser Polishing of Microfabricated Nickel Samples," Journal of Manufacturing Science and Engineering-Transactions of the Asme, vol. 131, no. 3, 2009.

[4] T. Gietzelt, O. Jacobi, V. Piotter, R. Ruprecht, and J. Hausselt,

"Development of a micro annular gear pump by micro powder injection molding," Journal of Materials Science, vol. 39, no. 6, 2004, pp. 2113-2119.

[5] S. Supriadi, E. R. Baek, C. J. Choi, and B. T. Lee, "Binder system for STS 316 nanopowder feedstocks in micro-metal injection molding," Journal of Materials Processing Technology, vol. 187, 2007, pp. 270-273.

[6] B. Y. Tay, L. Liu, N. H. Loh, S. B. Tor, Y. Murakoshi, and R. Maeda, "Surface roughness of microstructured component fabricated by [mu]MIM," Materials Science and Engineering A, vol. 396, no. 1-2, 2005, pp. 311-319.

[7] L. Liu, N. H. Loh, B. Y. Tay, S. B. Tor, Y. Murakoshi, and R. Maeda, "Effects of thermal debinding on surface roughness in micro powder injection molding," Materials Letters, vol. 61, no. 3, 2007, pp. 809-812.

[8] N. J. Hallab, K. J. Bundy, K. O'Connor, R. L. Moses, and J. J. Jacobs, "Evaluation of metallic and polymeric biomaterial surface energy and surface roughness characteristics for directed cell adhesion," Tissue Engineering, vol. 7, no. 1, 2001, pp. 55-71.

[9] P. F. Marella, D. B. Tuckerman, and R. F. Pease, "MODELING OF LASER PLANARIZATION OF THIN METAL-FILMS," Applied Physics Letters, vol. 54, no. 12, 1989, pp. 1109-1111.

[10] D. B. Tuckerman, and A. H. Weisberg, "Planarization of Gold and Alumunum Thin-Films using a Pulsed Laser," Ieee Electron Device Letters, vol. 7, no. 1, 1986, pp. 1-4.

[11] M. Bereznai, I. Pelsoczi, Z. Toth, K. Turzo, M. Radnai, Z. Bor, and A. Fazekas, "Surface modifications induced by ns and sub-ps excimer laser pulses on titanium implant material," Biomaterials, vol. 24, no. 23, 2003, pp. 4197-4203.

[12] A. Temmler, K. Graichen, and J. Donath, "Laser Polishing in Medical Engineering; Laser Polishing of Components for Left Ventricular Assist Devices," Laser Technik Journal, vol. 7, no. 2, 2010, pp. 53-57.

[13] Y. G. Kim, J. K. Ryu, D. J. Kim, H. J. Kim, S. Lee, B. H. Cha, H. Cha, and C. J. Kim, "Microroughness reduction of tungsten films by laser polishing technology with a line beam," Japanese Journal of Applied Physics Part 1-Regular Papers Short Notes & Review Papers, vol. 43, no. 4A, 2004, pp. 1315-1322.

[14] T. A. Mai, and G. C. Lim, "Micromelting and its effects on surface topography and properties in laser polishing of stainless steel," Journal of Laser Applications, vol. 16, no. 4, 2004, pp. 221-228.

[15] T. M. Shao, A. Hua, H. Y. Tam, and E. H. M. Cheung, "An approach to modelling of laser polishing of metals," Surface & Coatings Technology, vol. 197, no. 1, 2005, pp. 77-84.

[16] J. Martan, O. Cibulka, and N. Semmar, "Nanosecond pulse laser melting investigation by IR radiometry and reflection-based methods," Applied Surface Science, vol. 253, no. 3, 2006, pp. 1170-1177.

[17] W. E. Pendleton, G. P. Williams, R. T. Williams, J. C. Wu, G. B. Cvijanovich, J. L. Joyce, and M. McCleaf, "Scanning Tunneling Microscopy of Nickel Surface Features Before and After Rapid Melting by Excimer Laser," AMP Journal of Technology, vol. 3, 1993, pp. 75-84.

[18] K. Stout, and L. Blunt, Three-dimensional surface topography, Editor: 2000, pp. Pages.

[19] L. D. Landau, and E. M. Lifshits, Fluid mechanics, by L.D. Landau and E.M. Lifshitz, Editor: 1959, pp. Pages.

[20] V. N. Tokarev, and A. F. H. Kaplan, "An analytical modeling of time dependent pulsed laser melting," Journal of Applied Physics, vol. 86, no. 5, 1999, pp. 2836-2846.

[21] K. C. Mills, Recommended values of thermophysical properties for selected commercial alloys, Editor: 2002, pp. Pages.

[22] W. Zhang, C. H. Kim, and T. DebRoy, "Heat and fluid flow in complex joints during gas metal arc welding - Part I: Numerical model of fillet welding," Journal of Applied Physics, vol. 95, no. 9, 2004, pp. 5210-5219.

[23] M. Amara, V. Timchenko, M. El Ganaoui, E. Leonardi, and G. D. Davis, "A 3D computational model of heat transfer coupled to phase change in multilayer materials with random thermal contact resistance," International Journal of Thermal Sciences, vol. 48, no. 2, 2009, pp. 421-427.

[24] E. American Society of Mechanical, B. C. a. D. o. S. Q. American Society of Mechanical Engineers. Standards Committee, and I. American National Standards, Surface texture: surface roughness, waviness and lay, Editor: 2003, pp. Pages.

APPENDIX A: PLμP PARAMETERS

Stainless steel 316L	Type of laser	50 W CW/Modulated Fiber Laser
	Initial surface	Micro end-milling
	Pulse frequency (kHz)	20
	Pulse duration (ns)	5000
	Spot size (μm)	30
	Pulse energy (mJ)	0.040
	Melt duration (ns)	6820
	Critical frequency (mm^{-1})	40
Nickel	Type of laser	250 W CW Nd:YAG
	Initial surface	Macro scale grinding
	Pulse frequency (kHz)	4
	Pulse duration (ns)	650
	Spot size (μm)	60
	Pulse energy (mJ)	0.013
	Melt duration (ns)	994
	Critical frequency (mm^{-1})	145
Ti6Al4V	Type of laser	250 W CW Nd:YAG
	Initial surface	Micro end-milling
	Pulse frequency (kHz)	4
	Pulse duration (ns)	650
	Spot size (μm)	60
	Pulse energy (mJ)	0.036
	Melt duration (ns)	1164
	Critical frequency (mm^{-1})	115
Al-6061-T6	Type of laser	250 W CW Nd:YAG
	Initial surface	Macro scale grinding
	Pulse frequency (kHz)	4
	Pulse duration (ns)	650
	Spot size (μm)	60
	Pulse energy (mJ)	0.171
	Melt duration (ns)	2335
	Critical frequency (mm^{-1})	107